Ultrathin transition-metal oxide films: Thickness dependence of the electronic structure and local geometry in MnO

Mathias Nagel,[1,*] Indro Biswas,[1] Peter Nagel,[2] Eric Pellegrin,[2,†] Stefan Schuppler,[2] Heiko Peisert,[1] and Thomas Chassé[1]
[1]*Institute of Physical and Theoretical Chemistry, University of Tübingen, Auf der Morgenstelle 8, D-72076 Tübingen, Germany*
[2]*Forschungszentrum Karlsruhe, Institut für Festkörperphysik (IFP), D-76021 Karlsruhe, Germany*
(Received 26 January 2007; published 18 May 2007)

Ultrathin manganese monoxide films on silver substrates are studied as a function of the thickness using x-ray absorption spectroscopy and x-ray photoemission spectroscopy. By combining these techniques, an improved understanding of both the local geometry and the electronic structure is achieved. It was found that both electronic and geometric properties in ultrathin films differ significantly from the bulk. A tetragonal distortion of the oxide films is revealed by polarization-dependent x-ray absorption measurements; the extent is decreasing gradually with increasing film thickness. A relaxation of an epitaxial oxide layer induced by heating also leads to a decrease of the tetragonal interface strain. The electronic structure of ultrathin manganese oxide films changes in the valence-band region with dependence on thickness.

DOI: 10.1103/PhysRevB.75.195426 PACS number(s): 68.35.−p, 73.90.+f, 78.70.Dm, 79.60.Dp

I. INTRODUCTION

Binary transition-metal oxides have been attracting fundamental scientific interest for many years. Their strong electron-electron interaction combined with their compositional simplicity makes them important model compounds for understanding the effects of strong correlation in phenomena such as magnetism and electron transport. Novel properties are predicted for ultrathin films of these oxides on metallic substrates.[1] These properties are expected to differ from bulk properties due to both the reduced dimensionality and the influence of the interface. The metallic substrate may have a purely electronic contribution to the properties of ultrathin films by changing the electron density at the interface.[2] This may change either the ground state of the oxide film or the screening in response to an electronic excitation.[3,4] In case of less inert metallic substrates, interface reactions in various extent can take place.[5–9] Furthermore, interface strain effects may be observed in epitaxial layer systems with a lattice mismatch.[10] It is of basic interest whether these different influences can be used to tune the properties of ultrathin films systematically. Several studies have been carried out on NiO thin films on Ag (001) as well as on MgO (001) substrates. On the other hand, bulk samples of the oxides of the neighboring metals—CoO or MnO—have been extensively studied. It has been a long-time challenge for theoreticians to properly describe the experimental properties of MnO with calculations. This led to an improved understanding of the electronic—especially the insulating nature of MnO—and the structural and magnetic properties.[11–14] Thin films of the polar surfaces CoO (111) and MnO (111) as well as the nonpolar Co (001) surface on several metal substrates have been investigated regarding growth mode and electronic and structural properties with scanning tunneling microscopy, photoemission, and electron-diffraction techniques.[15–17] Ultrathin films of the nonpolar MnO (001) surface have been rarely studied.[18,19] The electronic and structural properties of ultrathin films of these binary monoxides need to be explored. In this study, we focus on ultrathin films of MnO on Ag (001). We chose silver as a substrate as it can be considered chemically inert. No detectable reactions take place at the present preparation conditions. The Ag (001) surface can be considered to be very close to the truncated fcc bulk structure (a=4.086 Å): No surface reconstructions are known and only a small relaxation of the topmost layers occurs.[20] Bulk manganese oxide has rocksalt structure with a lattice constant of a=4.445 Å at 300 K. Consequently, the lattice mismatch to the substrate is quite high (9%). Depending on the preparation parameters, substrate temperature, manganese flux, oxygen partial pressure and annealing time, i.e., both thermodynamic and kinetic conditions, films of good epitaxial quality can be obtained.[18] By choosing the optimal preparation method, it is possible for us to obtain either a film growth with a lattice match in the surface plane or relaxed growth of MnO on Ag (001). Here, we present results regarding both the electronic and local geometric properties as a function of the MnO film thickness.

II. EXPERIMENT

X-ray absorption (XAS) and photoelectron spectroscopy experiments were carried out at IFP's soft x-ray beamline WERA at the Karlsruhe synchrotron radiation facility ANKA. Epitaxial layers of MnO on a Ag (001) surface—with thicknesses in the range from 0.2 to 4 nm—were prepared stepwise *in situ* by thermal evaporation of manganese with a flux of 1.0 Å min^{-1} in a reactive oxygen atmosphere (2×10^{-7} mbar). The single-crystal substrate, orientation accuracy $<0.1°$ (MaTecK GmbH, Germany), was kept at 475 K during the film growth and during a successive annealing in ultrahigh vacuum (UHV) for 2 h. The base pressure inside the preparation chamber was 10^{-10} mbar and did not exceed 3.0×10^{-9} mbar during evaporation of pure manganese. The layer thickness was determined with a quartz microbalance referenced against x-ray photoemission spectroscopy (XPS) intensities of substrate and overlayer peaks using the closed layer model. A MnO (001) single crystal used as bulk reference (TBL-Kelpin, Germany) was cleaned

by several sputtering-annealing cycles (500 eV Ar^+ ion bombardment, 740 K). Photoelectron spectra (XPS) of the Mn $2p$, Mn $3s$, and O $1s$ core levels were measured to confirm the chemical state of the manganese and the stoichiometry. The epitaxial quality of the layers was monitored with low-energy electron diffraction (LEED). Soft x-ray photoelectron spectra in the valence-band region using a photon energy of 200 eV and an overall resolution of 150 meV were taken to study changes in the electronic properties as a function of the film thickness. An ultrathin 0.28 nm epitaxial layer was annealed at temperatures up to 600 K, leading to both relaxation of the film and island formation visible as specific changes in the LEED patterns. Polarization-dependent XAS spectra of the Mn $L_{2,3}$ edge were taken in total electron yield (TEY) and partial electron yield (PEY) detection modes for all layer thicknesses as well as for the cleaned MnO (001) reference crystal. The Mn $L_{2,3}$ PEY spectra were measured with a cutoff energy which was sufficient to completely suppress the contribution of oxygen (530 eV). The energy resolution was set to 100 meV for the XAS spectra. The degree of linear polarization for the angle-dependent measurements was set to 97%. The incident photon flux I_0 was monitored online with a gold mesh for background correction. All measurements were performed with the sample at room temperature, well beyond the bulk MnO Néel temperature of 118 K.

III. SIMULATIONS

The theoretical simulations of the Mn $L_{2,3}$ spectra were conducted with the software package TT-MULTIPLETS.[21–23] It is based on a full atomic multiplet calculation with a subsequent crystal-field splitting calculation. The spectra were calculated via a transition matrix between the ground-state configuration ($2p^6 3d^5$) and a final state ($2p^5 3d^6$) of a Mn^{2+} ion. In this study, we focused on this transition matrix; no further configurations like charge-transfer states were considered. The obtained line spectra were broadened with a Lorentzian of width 0.1 eV for the L_3 edge and of 0.3 eV for the L_2 edge and an overall Gaussian contribution of 0.15 eV full width at half maximum (FWHM). These broadening parameters lead to a good correlation between experimental and calculated bulk MnO spectra.[24] They were also used for the simulation of the Mn $L_{2,3}$ spectra taken from the ultrathin films. In the MnO bulk structure, manganese is sixfold coordinated by oxygen ligands with O_h symmetry. As shown in Fig. 1(a), the experimental Mn $L_{2,3}$ spectra of bulk MnO can be well reproduced by an atomic multiplet calculation with an additional octahedral crystal-field splitting of $10D_q$=0.85 eV. However, for the successful simulations of spectra from the epitaxial oxide films, a tetragonal distortion of the octahedral ligand sphere had to be taken into account for pseudomorphic growth (symmetry reduction from O_h to D_{4h}). The in-plane compression of epitaxial MnO on Ag (001) is accompanied by an elongation perpendicular to the substrate surface [see Fig. 1(b)]. This results in a splitting of the formerly degenerate t_{2g} and e_g orbitals and, consequently, to an angle dependence of the x-ray absorption spectra measured with linear polarized light. In the calculations, this splitting

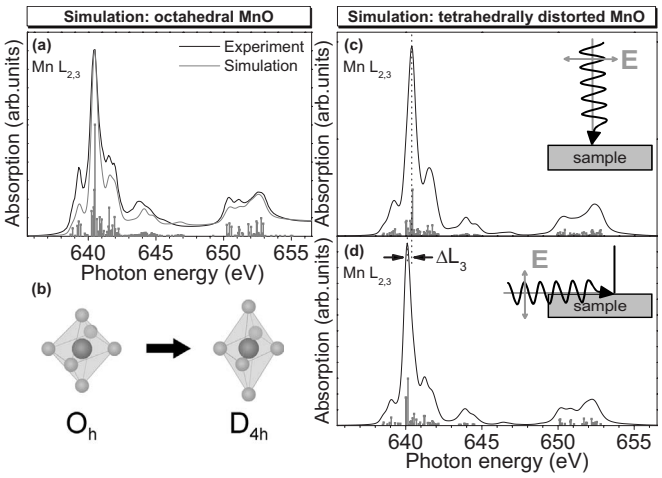

FIG. 1. (a) Experimental x-ray absorption (XA) spectrum of a MnO (001) bulk sample compared to the simulated spectrum. The simulation is based on an atomic multiplet calculation with a subsequent crystal-field splitting of $10D_q$=0.85 eV. The obtained line spectrum (gray bars) was broadened with a Lorentzian of width 0.1 eV for the L_3 edge and of 0.3 eV for the L_2 edge, and an overall Gaussian contribution of 0.15 eV FWHM. (b) Illustration of the tetrahedral distortion for a MnO_6 octahedron which is compressed *in-plane*. (c) Calculated Mn $L_{2,3}$ XA spectra of a distorted MnO_6 octahedron for *normal incidence*. (d) Calculated Mn $L_{2,3}$ XA spectra of a distorted MnO_6 octahedron for *grazing incidence*. The exact energy shift ΔL_3 is a main criterion to find the matching simulations for the experimental spectra.

was introduced via the additional crystal-field parameters D_s and D_t in addition to the octahedral crystal-field splitting parameter $10D_q$.[25] These parameters were varied from 0.80 to 0.90 eV for $10D_q$, from 0 to 110 meV for D_s, and from 0 to 5 meV for D_t, leading to a set of 414 simulations. Two model spectra were then calculated for each set of parameters: The first spectrum with an electric-field vector perpendicular to the axis of the tetragonal distortion (normal incidence) and the second with an electric-field vector parallel to the surface normal (grazing incidence) [see Figs. 1(c) and 1(d)]. Spectra of any given angle can be calculated as a geometrically weighted summation of these orthogonal spectra. The experimental spectra recorded at normal incidence and at 70° with respect to the surface normal were compared to simulated spectra in order to determine the crystal-field parameters for each film thickness. The first criterion for the selection of the corresponding simulation was the exact energy shift ΔL_3 of the main feature of the L_3 edge with the change of the polarization [see Figs. 1(c) and 1(d)]. The second criterion was the overall shape of the linear dichroism spectrum which changes in a characteristic manner with varying parameters. The linear dichroism spectrum results from subtracting the spectrum taken at 70° from the spectrum taken at 0°. Additionally, the distances between the features in the L_2 edge were taken into account. This method of selecting the appropriate parameter set allows us to give an estimation of the variation range for the crystal-field parameters, i.e., about 5–10 meV.

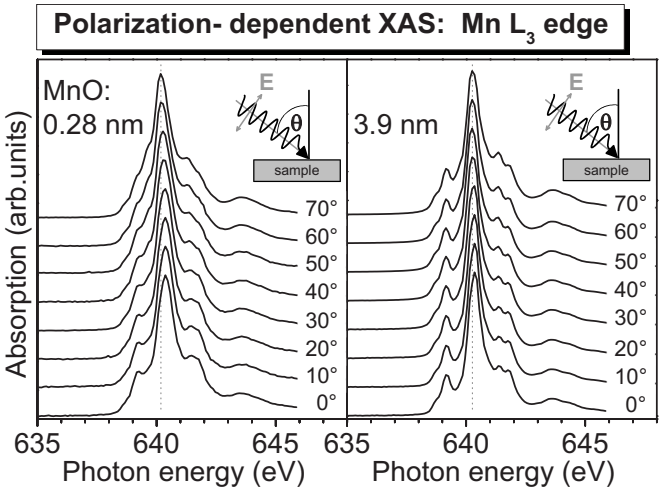

FIG. 2. Polarization-dependent Mn L_3 XA spectra of a 0.28 nm (left) and a 3.9 nm (right) MnO (001) film on Ag (001).

IV. RESULTS AND DISCUSSION

In the MnO bulk structure, manganese is octahedrally coordinated by oxygen. Therefore no polarization dependence is expected in the XAS spectra of the MnO (001) crystal, as confirmed by our measurements. The peak positions, the relative intensities, and the overall intensity after normalization with respect to the edge jump remain unchanged for the reference crystal when going from normal to grazing incidence. In contrast to this, clear changes in the peak positions and the relative intensities are visible in the polarization-dependent Mn $L_{2,3}$ edge spectra of the ultrathin films. These changes become evident in different angular-dependent sets of spectra recorded at the different film thicknesses (see Fig. 2).

The most prominent change is the shift of the main peak of the L_3 edge to lower energies when going from normal to grazing incidence. We observe that the polarization-dependent energy shift of the main feature in the L_3 edge depends systematically on the film thickness of the oxide layer. The ΔL_3 values change, e.g., from −210 meV for the 0.28 nm film thickness to −100 meV for the 3.9-nm-thick film. The two features in the region between 641 and 642 eV show a significant polarization-dependent change in their relative intensities. Additionally, we find that the spectral contribution in the region between 639 and 640 eV increases in the series from 0° to 70°. Especially for the 0.28-nm-thick film, the features that are visible as separated satellites beside the main peak of the L_3 edge are diminished to a shoulder. When we compare the spectral series of the 0.28- and 3.9-nm-thick films, we find that the spectral features of the thicker film are sharper (see Fig. 2). The broadened features in the spectra of the low film thicknesses might be an indication of a reduced film homogeneity. However, this broadening is also present in our calculations (see discussion below) and is regarded as a consequence of the changes in the crystal field. The spectra of the 3.9-nm-thick film look already very similar to the spectra of bulk MnO (001). However, the change of the polarization still leads to a shift of the main feature in the L_3 edge of about 100 meV. These

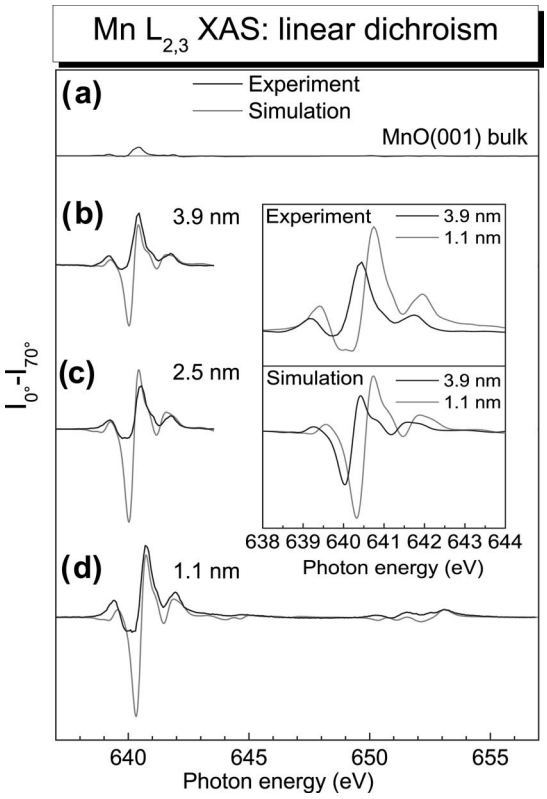

FIG. 3. Linear dichroism of the Mn $L_{2,3}$ x-ray absorption spectra of (a) a MnO (001) single crystal, (b) a 3.9 nm MnO (001) film on Ag (001), (c) a 2.5 nm MnO (001) film on Ag (001), and (d) a 1.1 nm MnO (001) film on Ag (001). The experimental spectra (black solid curves) are directly compared to the theoretical simulations (dashed gray curves). The inset shows the experimental and theoretical findings of the L_3 edge for two different film thicknesses. The theoretical spectra are scaled with a factor of 10 to fit the experimental intensities.

angular-dependent changes can be studied in more detail in linear dichroism (LD) plots. For this purpose, we subtracted the normalized spectra taken at an angle of 70° from the spectra at 0° and plotted them together with the related simulations scaled by a factor of 10 to match the total intensity (see Fig. 3). The LD plot of the bulk MnO shows only a small artifact at the position of the highest absorption intensity. This might originate from saturation effects in the bulk oxide which cannot be completely corrected (for details of this procedure, see Ref. 26 and references therein). In the LD plots we see that the dichroism decreases and that features shift to lower energies with increasing film thickness. Our simulations closely resemble these experimental findings, as can be seen in more detail in the inset of Fig. 3.

In our simulations we assume that the epitaxially grown manganese oxide layers on a silver substrate are tetrahedrally distorted MnO_6 octahedrons. This describes the observed linear dichroism reasonably well. The influence of the substrate on the layer decreases with increasing film thickness. Consequently, we expect that the distortion of the MnO structure by the matching to the Ag substrate decreases with increasing film thickness. In general, the influence of the substrate on the distortion of the epitaxial layer can be discussed in

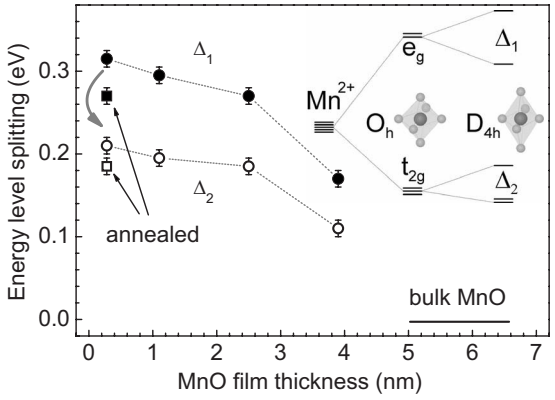

FIG. 4. The tetragonal orbital splitting values Δ_1 (black closed circles) and Δ_2 (black open circles) decrease with increasing film thickness. The black line on the lower right-hand side shows a film thickness for a bulklike behavior, i.e., an undistorted crystal field can be expected. The inset shows the tetragonal distortion of the crystal field caused by an in-plane compression of the epitaxial oxide film. Heating of a 0.28 nm epitaxial layer (gray arrow) leads to a decrease of the distortion and thus to a decrease of the tetragonal orbital splitting (black squares).

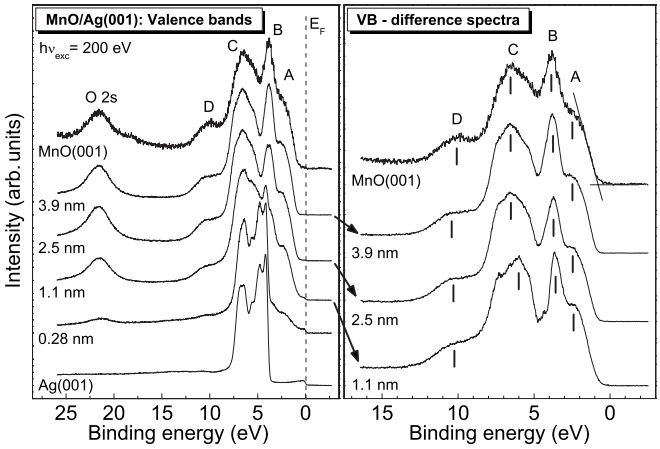

FIG. 5. Valence band (left) and valence-band difference spectra (right) of the ultrathin MnO films (gray), the silver substrate, and the MnO (001) reference (black). The binding energy of the thin-film spectra can be precisely aligned with the Fermi edge of the subjacent silver before subtraction (dotted line). The bulk MnO spectrum can be aligned with the O 2*s* peak at 21.4 eV. In the MnO (001) spectra, we show the method used to determine the valence-band maximum (black lines). The positions of the features A, B, C, and D are indicated by the black bars. Especially for feature A and B, a significant shift is visible with increasing film thickness.

different ways. The simplest model to describe the distortion within the oxide layer is the assumption of a homogeneously deformed layer for each film thickness. Alternatively, one can assume the spectra of an oxide layer to be composed of a homogeneously distorted layer with a contribution of the topmost layer in which manganese has a crystal field with C_{4v} symmetry. A more advanced model would include a gradual change of the distortion within the layer. However, we did not find any differences between the spectra of the 3.9-nm-thick film recorded with TEY, probing a depth of about 5–10 nm and thus the entire ultrathin film, and with PEY, probing a depth in the few nanometer range. Therefore the latter two contributions are less likely. This separation into surface- and bulk-sensitive probing might not hold for the lowest thicknesses since both recording methods should probe the entire film. Consequently, the crystal-field distortion parameters for these samples might be averaged values. An experimental indicator for this assumption can be the slightly increased linewidth compared to the related simulation. Having identified the tetragonal distortion as the main origin of the spectral changes, we find a clear trend with increasing film thickness (see Fig. 4). The orbital splitting values of the e_g and t_{2g} orbitals in a tetragonal crystal field, Δ_1 and Δ_2, respectively, decrease with growing film thickness. By extrapolating this trend to a nondistorted crystal field, we expect purely bulklike manganese oxide films to set in at about 5 nm thickness. In addition, we found that the distortion decreases when epitaxially grown MnO is forced to relax by heating the sample up to 600 K, as shown for the 0.28 nm layer. XPS core-level intensity ratios of the heated 0.28 nm layer have been analyzed using a peak shape analysis software[27] in order to obtain information on the changes of the surface composition. The peak intensity ratio of the Ag 4*s* peak to the Mn 3*s* doublet changes from approximately 2:1 for the epitaxial film to 4:1 for the annealed film. The mean free paths for electrons can be considered to be equivalent for both levels. The increase of this ratio demonstrates a redistribution of MnO at the surface, very likely accompanied by island formation.

In order to compare these thickness-dependent changes observed in XAS with spectra which give information about occupied states, we conducted photoemission experiments. The valence-band (VB) spectra are shown in Fig. 5 (left). Changes in the VB region of ultrathin MnO on silver are not directly observed with XPS, since the Ag 4*d* bands with maxima located at 4.8 and 6.3 eV mask the MnO features, especially at very low film thickness. The Fermi edge of the silver substrate is still visible in the ultrathin film spectra. By subtracting a scaled reference spectrum of the clean silver surface, the valence-band region of ultrathin MnO films can be revealed [see Fig. 5 (right)]. The intensity scaling before subtraction has been performed by aligning the Fermi edges of the clean substrate spectrum and the thin-film spectrum.

After subtracting the silver reference spectrum, we observe four dominant features A, B, C, and D in the VB of ultrathin MnO films, as reported recently for bulk MnO.[28] Even for the lowest film thicknesses, these features are observed in the spectrum. However, there are some changes in the relative intensities and energy positions. The valence-band maximum is shifted from 0.8 to 0.5 eV, going from bulk MnO to the ultrathin film of 0.28 nm thickness. Thus, the Fermi level appears closer to the valence-band maximum in the thin-film case. Also feature B shifts from 3.9 to 3.5 eV. Within feature C, spectral weight is shifted from higher to lower binding energies. Feature D hardly changes in its intensity. The origin of the four features has been discussed controversially. Calculations on the basis of the ligand field theory combined with the configuration-interaction (CI) approach were performed to resemble the experimental spectra.[11–13,29] *Ab initio* studies with the PBE

$+U$ approach have been recently utilized to successfully derive the properties of the MnO (001) surface.[14] As an outcome from CI calculations, features A and B can be attributed to ${}^5E_g$ and ${}^5T_{2g}$ symmetry states respectively, after removal of a Mn $3d$ electron. The amount of mixing between d^4 and $d^5\underline{L}$ final states is under debate and is discussed to be up to 50%. According to Ref. 13 feature C gains about 18% intensity from a 4 eV broad O $2p$ band. Preceding calculations suggest a broad O $2p$ band which is split into σ and π bonding orbitals, whereas the π bonding part also contributes to feature B. According to the density of states *ab inito* calculation in Ref. 14 Mn $3d$ and O $2p$ states contribute to the overall VB but with different weights than found for CI calculations. On the one hand, the origin of feature D is discussed in terms of intrinsic contributions due to configuration interaction as calculated by van Elp *et al.*[13] and as derived experimentally by Lad and Heinrich[11] in analogy to NiO CI calculations. On the other hand, spectral weight in this region is ascribed to manganese vacancies, impurities, or oxygen defects by Fujimori *et al.*[12] based on their calculations. The assumption of manganese vacancies as an origin for feature D is supported experimentally by Jeng *et al.*[30] It is also worth noting that the difference spectra of the ultrathin films show a decreasing spectral contribution in the region between features C and D with increasing film thickness. This observation fits both interpretations of the origin of spectral weight in this region, since we might expect more vacancies in ultrathin films than for bulklike films. Nonlocal contributions are caused by charge transfers from the coordinating ligand sphere to the metal atom or by even more delocalized charge redistributions. Therefore the presence of nonlocal contributions, as described with CI calculations, should be slightly increased for defect-free films or films with larger domains of ordering. The difference spectra may contain small artifacts of the subtraction procedure. Especially the difference spectrum of the 0.28-nm-thick film is susceptible to artifacts in the range from 3.8 to 7.5 eV due to the high spectral contribution of silver states in this region. Nevertheless, the observed changes remain significant and show a trend for increasing film thickness. Two reasons for these changes may be considered. An influence of the tetragonal distortion as probed with XAS is possible. On the other hand, ground-state and final-state effects due to the silver substrate may also have to be taken into account.[1] This calls for a more detailed theoretical analysis.

V. CONCLUSION AND OUTLOOK

We have clearly observed that the change in the electronic structure of ultrathin MnO films on Ag (001) is thickness dependent as a consequence of the change of the local geometry around the manganese atom. The results from the Mn $L_{2,3}$ x-ray absorption spectra give evidence for a decrease of the tetragonal distortion with increasing film thickness. The valence-band photoemission spectra of ultrathin MnO films closely resemble those of the bulk material. Significant thickness-dependent changes are revealed in the difference spectra. These findings are of interest for investigations in which thin metal-supported oxide films are prepared to mimic bulklike properties. On the other hand, one can use the thickness-dependent changes to tailor electronic properties of thin films gradually. Further investigations will follow to study the influence of the oxide layer thickness on other properties such as magnetic phenomena.

ACKNOWLEDGMENTS

We acknowledge the ANKA Angstroemquelle Karlsruhe for the provision of beamtime at the beamline WERA. We thank F. de Groot for providing the simulation software TT-MULTIPLETS and for helpful discussions.

*Present address: Institute of Physical and Theoretical Chemistry, University of Tübingen, Auf der Morgenstelle 8, D-72076 Tübingen, Germany. Electronic address: mathias.nagel@uni-tuebingen.de. URL: http://www.uni-tuebingen.de/chasse/

†Present address: ALBA Synchrotron Light Source, Apartado de correos 68, E-08193 Bellaterra, Spain.

[1] S. Altieri, L. H. Tjeng, and G. A. Sawatzky, Thin Solid Films **400**, 9 (2001).

[2] A. M. Ferrari, Surf. Sci. **584**, 269 (2005).

[3] S. Altieri, L. H. Tjeng, F. C. Voogt, T. Hibma, and G. A. Sawatzky, Phys. Rev. B **59**, R2517 (1999).

[4] S. Altieri, L. H. Tjeng, F. C. Voogt, T. Hibma, O. Rogojanu, and G. A. Sawatzky, Phys. Rev. B **66**, 155432 (2002).

[5] R. de Masi, D. Reinicke, F. Müller, P. Steiner, and S. Hüfner, Surf. Sci. **515**, 523 (2002).

[6] T. J. Regan, H. Ohldag, C. Stamm, F. Nolting, J. Lüning, J. Stöhr, and R. L. White, Phys. Rev. B **64**, 214422 (2001).

[7] S. Benedetti, P. Luches, M. Liberati, and S. Valeri, Surf. Sci. **572**, L348 (2004).

[8] M. Nagel, L. Zhang, H. Peisert, and T. Chassé, Microchim. Acta **156**, 27 (2006).

[9] S. Krasnikov, A. Vinogradov, K.-H. Hallmeier, R. Höhne, M. Ziese, P. Esquinazi, T. Chassé, and R. Szargan, Mater. Sci. Eng., B **109**, 207 (2004).

[10] M. W. Haverkort, S. I. Csiszar, Z. Hu, S. Altieri, A. Tanaka, H. H. Hsieh, H.-J. Lin, C. T. Chen, T. Hibma, and L. H. Tjeng, Phys. Rev. B **69**, 020408(R) (2004).

[11] R. J. Lad and V. E. Henrich, Phys. Rev. B **38**, 10860 (1988).

[12] A. Fujimori, N. Kimizuka, T. Akahane, T. Chiba, S. Kimura, F. Minami, K. Siratori, M. Taniguchi, S. Ogawa, and S. Suga, Phys. Rev. B **42**, 7580 (1990).

[13] J. van Elp, R. H. Potze, H. Eskes, R. Berger, and G. A. Sawatzky, Phys. Rev. B **44**, 1530 (1991).

[14] V. Bayer, C. Franchini, and R. Podloucky, Phys. Rev. B **75**, 035404 (2007).

[15] S. Sindhu, M. Heiler, K.-M. Schindler, W. Widdra, and H. J. Neddermeyer, Surf. Sci. **566-568**, 471 (2004).

[16] C. Franchini, V. Bayer, R. Podloucky, G. Parteder, S. Surnev, and F. P. Netzer, Phys. Rev. B **73**, 155402 (2006).

[17] G. A. Rizzi, M. Petukhov, M. Sambi, R. Zanoni, L. Perriello, and

G. Granozzi, Surf. Sci. **482-485**, 1474 (2001).
[18] F. Müller, R. de Masi, D. Reinicke, P. Steiner, S. Hüfner, and K. Stöwe, Surf. Sci. **520**, 158 (2002).
[19] M. Nagel, I. Biswas, H. Peisert, and T. Chassé, Surf. Sci. (to be published).
[20] H. Li, J. Quinn, Y. S. Li, D. Tian, F. Jona, and P. M. Marcus, Phys. Rev. B **43**, 7305 (1991).
[21] F. M. F. de Groot, J. C. Fuggle, B. T. Thole, and G. A. Sawatzky, Phys. Rev. B **42**, 5459 (1990).
[22] R. D. Cowan, J. Opt. Soc. Am. **58**, 808 (1968).
[23] P. H. Butler and B. G. Wybourne, Int. J. Quantum Chem. **10**, 581 (1976).
[24] F. M. F. de Groot, J. Electron Spectrosc. Relat. Phenom. **67**, 529 (1994).
[25] F. M. F. de Groot, Coord. Chem. Rev. **249**, 31 (2005).
[26] S. Gota, M. Gautier-Soyer, and M. Sacchi, Phys. Rev. B **62**, 4187 (2000).
[27] R. Hesse, T. Chassé, and R. Szargan, Anal. Bioanal. Chem. **375**, 856 (2003).
[28] F. Parmigiani and L. Sangaletti, J. Electron Spectrosc. Relat. Phenom. **98-99**, 287 (1999).
[29] D. E. Eastman and J. L. Freeouf, Phys. Rev. Lett. **34**, 395 (1975).
[30] S.-P. Jeng, R. J. Lad, and V. E. Henrich, Phys. Rev. B **43**, 11971 (1991).